# Adiabatic versus conductive heat transfer in off-critical $SF_6$ in the absence of convection

T. Fröhlich, P. Guenoun, M. Bonetti, F. Perrot, and D. Beysens*
*Commissariat à l'Energie Atomique (CEA), Centre d'Etudes de Saclay, Service de Physique de l'Etat Condensé (SPEC), F-91191 Gif-sur-Yvette Cedex, France*

Y. Garrabos
*Institut de Chimie de la Matière Condensée de Bordeaux (ICMCB), Université Bordeaux I, F-33600 Pessac, France*

B. Le Neindre
*Laboratoire d'Ingénierie des Matériaux et des Hautes Pressions (LIMHP), Université de Paris Nord, F-93430 Villetaneuse, France*

P. Bravais
*L'Air Liquide, F-38360 Sassenage, France*
(Received 27 December 1995; revised manuscript received 13 March 1996)

The process of adiabatic heating of compressible fluids [piston effect (PE)] has been investigated in $SF_6$ at off-critical density $\rho \approx 1.27\rho_c$ near the coexistence temperature in the absence of convection. The temperature response of the fluid to an internal heat pulse has been recorded at different distances from the heat source confirming a (spatially) homogeneous temperature rise outside an expanding boundary layer during heating. This process can be distinguished from the following conductive heat transfer when the energy contained in the boundary layer diffuses. This observation is confirmed by both experiment and calculations. During and after the heating process, $(P,\rho,T)$ data of the fluid behaves according to a given equation of state at equilibrium because hydrodynamic velocities remain small. The isentropic character of the PE was confirmed by both calculations from the pressure and density measurements. The presented experimental results were obtained on ESA's critical point facility (CPF) during the Spacelab IML-2 mission in July 1994. [S1063-651X(96)04507-2]

PACS number(s): 44.10.+i, 05.70.Jk, 66.10.Cb

## I. INTRODUCTION

The transport of heat in dense pure fluids classically involves the mechanisms of convection, diffusion, and radiation. Recently, the understanding of thermal equilibration of a pure fluid near its gas-liquid critical point (CP) has evidenced a fourth mechanism, the so-called ''piston effect'' (PE) [1–7]. Although it is also present in an ideal gas [4], it is emphasized near the CP where the compressibility of a fluid diverges. This high compressibility leads to an unstable character of supercritical fluids which induces buoyancy-driven convection in the presence of an accelerating field (gravitation, rotation, . . . ). To suppress these perturbing convective flows and carry out a proper experimental analysis of the different modes of heat transfer, a microgravity environment has been used.

When such a supercritical homogeneous fluid enclosed in a sample cell is suddenly heated from one wall, a diffusive thermal boundary layer [''hot boundary layer'' (HBL)] forms at this wall-fluid interface. Due to the high compressibility of the fluid outside the layer (''bulk''), the fluid layer expands and acts as a piston, generating an acoustic wave which propagates in the bulk and which is reflected on the second wall enclosing the fluid. Thermal conversion of this pressure and density rise is, in turn, able to heat the fluid in an adiabatic way. As a result, spatially uniform heating of the bulk fluid occurs on an acoustic time scale $t_a = L/c$ (with $L$ the characteristic sample dimension and $c$ the sound velocity in the fluid). During repeated travels of the pressure wave in the fluid, the bulk temperature progressively rises to reach thermal equilibrium. At the same time, heat starts to diffuse from the fluid into the nonheated walls, if these are not perfectly isolating. In this case, a ''cold'' boundary layer (CBL) is formed at this interface, where the fluid contracts and thus decompresses the bulk. It is then the competition between the HBL and the CBL which rules the evolution of the bulk fluid state.

When deriving the energy balance for heat transfer in a compressible medium, the pressure term has to be taken into account and we obtain

$$\frac{\partial T}{\partial t} = \frac{1}{\rho c_P}\frac{1}{r^n}\frac{\partial}{\partial r}\left(r^n \lambda \frac{\partial T}{\partial r}\right) + \left(1 - \frac{c_v}{c_P}\right)\left(\frac{\partial T}{\partial P}\right)_\rho \frac{dP}{dt}. \quad (1)$$

Here, $\lambda$ is the thermal conductivity and $c_P$ and $c_v$ are the heat capacities at constant pressure and volume, respectively. The parameter $n$ indicates the geometry of the considered process and equals 0 for plane, 1 for cylindrical, and 2 for spherical geometry. Critical divergence of these properties induces a nonlinear diffusion process [5] coupled with adiabatic heating. In fact, this form of the energy equation stresses the two different types of heat transfer, which are the nonisentropic heat diffusion (first right-hand term) and the temperature variation due to isentropic compression (second term).

*Present address: Commissariat à l'Energie Atomique (CEA), Centre d'Etudes de Grenoble, Département de la Recherche sur la Matière Condensée (DRFMC), F-38054 Grenoble Cedex 9, France.

 

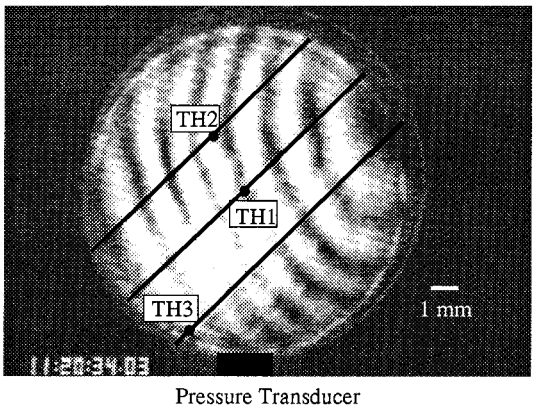


FIG. 1. The interferometry sample cell in a homogeneous state. Note the distribution of thermistors TH1–TH3 and the pressure transducer. The curvature of the fringes is not due to density gradients.

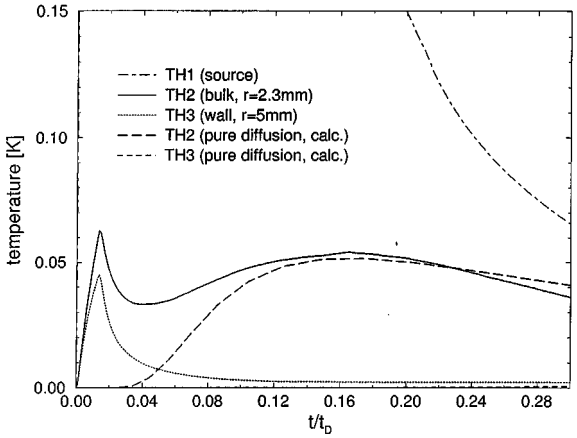


FIG. 2. The temperature response of the three thermistors on a 15 s heat pulse is traced over time where time is plotted in units of the diffusion time. The calculated result of a purely diffusive heat transport is given for TH2 and TH3 for comparison (see text).

Note that

$$\left(1-\frac{c_v}{c_P}\right)\left(\frac{\partial T}{\partial P}\right)_\rho=\left(\frac{\partial T}{\partial P}\right)_s . \tag{2}$$

The influence of this term grows as the CP is approached because of the divergence of the heat capacity $c_P$. In our experiment, hydrodynamic velocities are very small ($\leqslant$1 mm/s) and can be neglected when analyzing the PE heat transfer. In this case, Eq. (1) is sufficient to model the thermalization process. For an additional investigation of the thermo-acoustic origin (i.e., the propagation of the sound waves) or when taking viscous dissipation into account, a numerical simulation of the Navier-Stokes equations is necessary. This has been done for a one-dimensional (1D) van der Waals gas in [6,7].

The goal of this study is to provide unambiguous, distinctive measurements of these two modes of heat transport in the same sample and to check the theory of adiabatic heating by thermodynamic calculations. For this purpose, a supercritical sample at high, liquidlike density has been chosen. Such a sample also modelizes cryogenic reservoirs which are used for the storage of supercritical fluids in satellites and space vehicles, for example.

## II. EXPERIMENT

### A. Experimental setup

The experimental sample cell was of cylindrical shape (11.9 mm diameter, 6.67 mm thickness) and filled with $SF_6$ at the off-critical density $\rho\approx1.27\rho_c$ (Fig. 1). Radial walls were made of CuCoBe, whereas the sample was closed at the bottom and the top by sapphire windows. The sample was mounted into one arm of a Twymann-Green interferometer, interference fringes allowing the detection and analysis of density variations of the fluid. Density changes of the fluid are coupled to a variation of its refractive index $n$ as given by the Lorentz-Lorenz equation. This variation of $n$ induces a phase shift of the light beam proportional to the density changes. The light beam traverses the sample thickness two times, integrating the phase shift resulting from density variations of the fluid.

Additionally, three thermistors (Thermobeads B10, Thermometrics Inc.) were used to monitor the temperature at three different points of the sample. One of them TH1 was located in the middle of the sample and could be heated in order to perform an energy pulse within the fluid. The second thermistor TH2 was located at nearly half the distance between the source and the wall and TH3 near the thermostated wall. A pressure transducer integrated into the sample wall enabled measurements of pressure variations. During acquisition sequences, temperature measurements were sampled at a frequency of 1 Hz, while pressure was detected at 20 Hz and video images recorded at 30 Hz. The temperature stability of the thermostat was assured within 100 $\mu$K over several hours.

### B. Results and discussion

In our experiment, a series of 39 heat pulses of different duration has been carried out within the temperature range $T_{c,x}+100\ \text{mK}<T_i<T_{c,x}+2$ K. In the following, we concentrate our study on the case of a heat pulse of 15 s at an initial temperature $T_i\approx T_{c,x}+1$ K. Equivalent results as presented hereafter are obtained by analyzing the other pulses. Figure 2 shows the temperature response as measured by the three thermistors. One clearly distinguishes two temperature maxima in the curve sampled at TH2. The first one is due to PE heating, and we note that this process induces nearly the same signal amplitude on TH3. This evidences the homogeneity of heating by adiabatic compression which reaches the maximum value at the end of the pulse. Second, after pressure and temperature decrease, the diffusive temperature front propagating from the source (TH1) into the bulk reaches TH2. The time necessary for this process is of the order of the diffusive time $t_D=R^2/D$, where $R$ is a characteristic length of the diffusion process (here naturally the distance TH1-TH2) and $D$ the coefficient of diffusion. This second temperature maximum is not observed at TH3, because heat has diffused below the detection threshold before

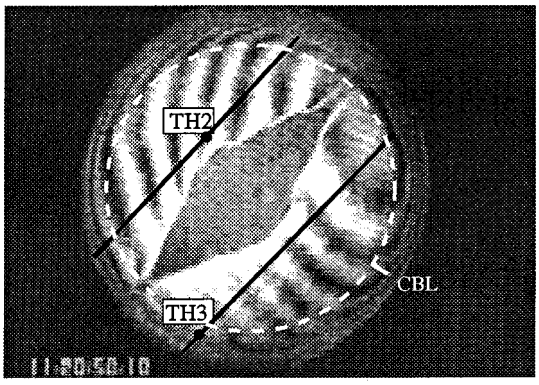


FIG. 3. The sample cell at the end of a 15 s heat pulse. Note that the HBL (gray diffusive zone) has not reached TH2 yet. As indicated by the strong curvature of the fringes, a CBL of thickness 0.6–0.8 mm has developed at the Cu-Co-Be wall.

reaching the more distantly located thermistor. The temperature difference ($T_{TH2}-T_{TH3}$) increases with time which is a demonstration of the development of a CBL diffusing from the thermostated CuCoBe walls. This layer progressively reaches TH3 and slows down the thermistor's temperature rise. The calculated result of an ideal, purely conductive heat transfer is added to the experimental curves, showing clearly that the diffusive temperature front does not have the time to reach TH2 within the heating period and that even for late stages no significant temperature increase is detected at TH3. The signal recorded with TH2 is then the isentropic temperature rise by PE heating. We note the following points in support of this claim: first, the video images of the interference pattern confirm that the diffusive region does not reach TH2 within the heating time (Fig. 3); second, it is obvious that the CBL does not influence TH2. The strong fringe curvature near the cell wall is a sign of the density gradient inside the CBL. At $t=15$ s, a CBL of thickness 0.6–0.8 mm can be detected (Fig. 3).

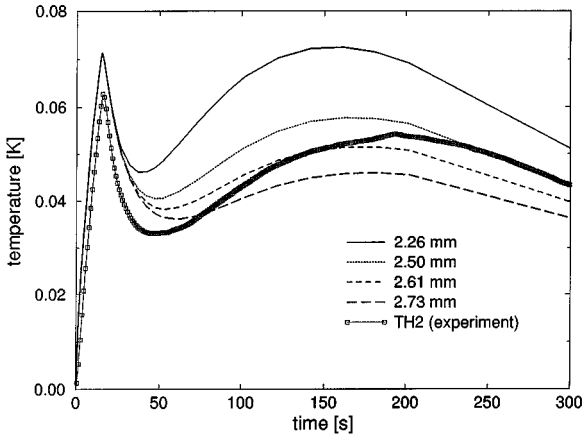


FIG. 4. The experimental temperature curve as measured by TH2 during and after a heat pulse of 15 s is compared with a numerical model. The fluid temperature at different distances from the heat source is traced over time. The model enables us to recover the general trends, i.e., a peak of adiabatic heating followed by a broader diffusive heating maximum.

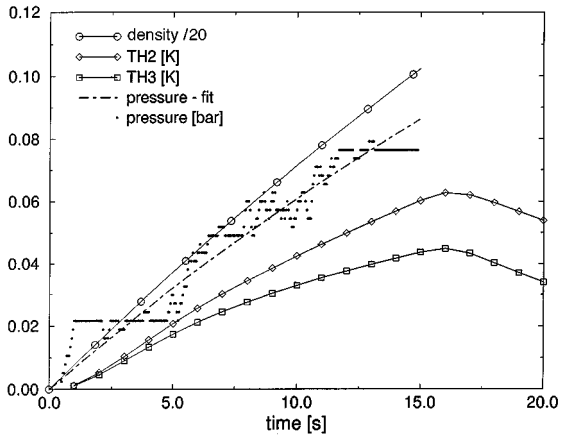


FIG. 5. Experimental temperature, pressure, and density changes during the heating period of 15 s are given as a function of time. Pressure is fitted by a second-order polynomial function. Density is considered to be homogeneous outside the HBL region.

Temperature curves obtained from a different calculation using a finite-element code are presented in Fig. 4 [8]. This model includes approaches to the case of a ''real'' experiment, e.g., the heat losses via the thermistor threads and at the cooling surface are taken into account. The calculation is axisymmetric and does not reproduce exactly the thermal characteristics of the cell materials. Therefore it does not allow us to fit the experimental data with precision but enables us to recover the involved mechanisms. The temperature evolution of fluid elements at different distances from the heat source (TH1) is shown during and after heating and compared with the experimental curve of TH2. From the solution of Eq. (1), the two temperature maxima at TH2 can be recovered within a good approximation for a distance TH1-TH2$\approx$2.5 mm which is close to the experimental setup ($\approx$2.3 mm). A magnification of the first 20 s of Fig. 2 is given on Fig. 5, where the pressure rise and the density evolution outside the HBL have been added to TH2 and TH3. In order to verify the isentropic character of PE heating, we calculate the corresponding temperature change from these density and pressure measurements by applying a linear transformation

$$\delta T=\left(\frac{\partial T}{\partial \rho}\right)_s \delta\rho \tag{3}$$

and

$$\delta T=\left(\frac{\partial T}{\partial P}\right)_s \delta P, \tag{4}$$

respectively. For this purpose, we evaluated first the isentropic partial derivatives in Eqs. (3) and (4) from an equation of state given by Abbaci and Sengers [9]. The corresponding isentropic temperature changes were then calculated and compared in Fig. 6 with the temperature response of TH2. To reduce the noise of the signal, we made use of the pressure fit in Fig. 5 when calculating the isentropic temperature $T(P)|_s$. It can be seen that the pressure coefficient $(\partial T/\partial P)_s$ gives much better results than the derivative with respect to density $(\partial T/\partial \rho)_s$ when assuming a homogeneous density

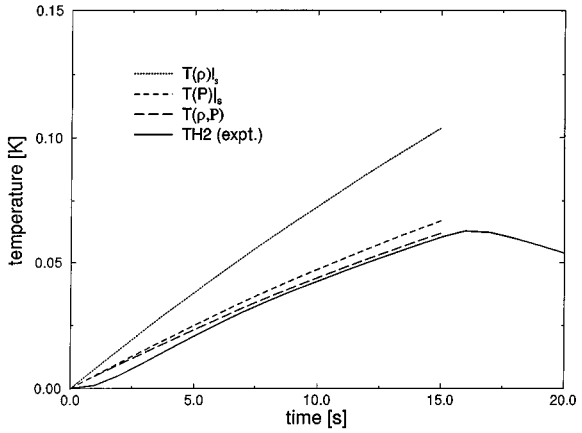


FIG. 6. The temperature rise measured at TH2 during a heat pulse of 15 s is compared with the calculated isentropic temperature variations and the equation of state [9]. Density-based calculations are not in agreement with the other three temperatures when assuming constant density outside the HBL region.

profile outside the HBL. A comparison of the temperature measurement with the equation of state is also given. Following density and pressure variations relative to an initial state of the fluid before heating, we trace the temperature evolution of the bulk fluid according to [9]. Good agreement with the experimental data is obtained.

In a following step, the two isentropic coefficients $(\partial T/\partial \rho)_s$ and $(\partial T/\partial P)_s$ have been derived from the experimental curves of different heat pulses within the temperature range $T_{c,x}+100$ mK$<T_i<T_{c,x}+2$ K. The heat pulses have been selected in order to show minimum convective displacement of the HBL. The coefficients are determined after approximately 10 s of heating to suppress any influence of the diffusive temperature front (Fig. 2). The experimental results are compared in Figs. 7 with the coefficients obtained from the equation of state. A systematic error of 50–100% is obtained for the density coefficient [Fig. 7(a)] where we consider again a homogeneous density profile in the region outside the HBL. A similar result has been previously found by Michels for $SF_6$ at critical density [10]. In contrast, the pressure coefficient gives better results, as already shown in Fig. 6. A value close to the one derived from Abbaci and Sengers' equation is found within the precision of the pressure measurement [Fig. 7(a)].

In what follows, we demonstrate that the discrepancy of the density measurements with the equation of state can be corrected. This correction is based on an analysis of the density profile throughout the sample thickness. In the case of an adiabatic sample, there are no temperature and density gradients in the bulk fluid outside the HBL and the phase shift corresponds to the homogeneous density increase according to PE compression of the bulk. The density measurements presented above were obtained under this assumption.

In contrast, in our experiment, the radial CuCoBe wall and sapphire windows remain very close to the initial temperature $T_i$ and can therefore be considered as isothermal. In order to estimate the maximum error coming from this assumption, a numerical simulation has been performed in which all walls act with the thermodynamic properties of the sapphire windows. At a distance inside the wall equal to the

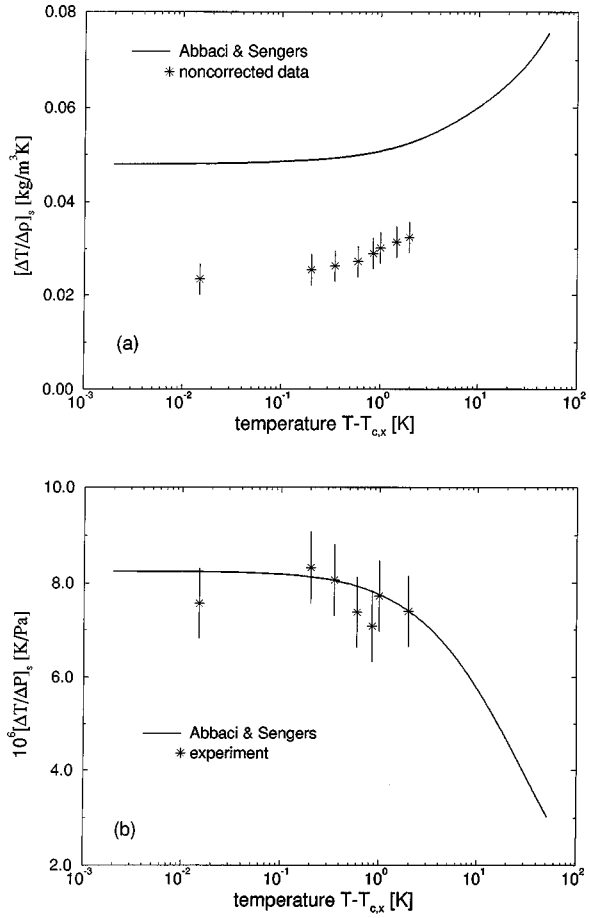


FIG. 7. The isentropic coefficients $(\partial T/\partial \rho)_s$ and $(\partial T/\partial P)_s$ obtained from the experiment are compared with the values derived from [9]. A discrepancy of 50–100% can be stated for the density coefficient when assuming a constant density profile in the fluid outside the HBL region (a). Good agreement is obtained for the pressure coefficient within the precision of pressure measurements (b).

real window thickness, the sample is considered as adiabatic. This suppression of any heat loss at the outer shell (external limits of the cell) will give us the upper limit of a possible temperature rise inside the sapphire windows during a heat pulse. We find that at the internal interface window (wall) fluid, the temperature increase of the wall remains smaller than 4% of the bulk temperature rise, e.g., $\approx$2.1 mK for a heating time of 15 s. This confirms that our assumption of an isothermal CuCoBe wall and sapphire windows is justified.

The fluid temperature profile of the CBL is then a convolution of the temperature evolution of the bulk fluid and the error function describing the response to an ideal temperature step

$$\delta T(x,t) = T(x,t) - T_{\mathrm{TH2}}(t) = \frac{d[T_i - T_{\mathrm{TH2}}(t)]}{dt} \otimes \mathrm{erfc}\left(\frac{x}{2\sqrt{Dt}}\right). \quad (5)$$

Here, $x$ is the spatial coordinate in direction of the sample thickness and erfc the inverse error function. The position $x=0$ corresponds to the window-fluid interface where the

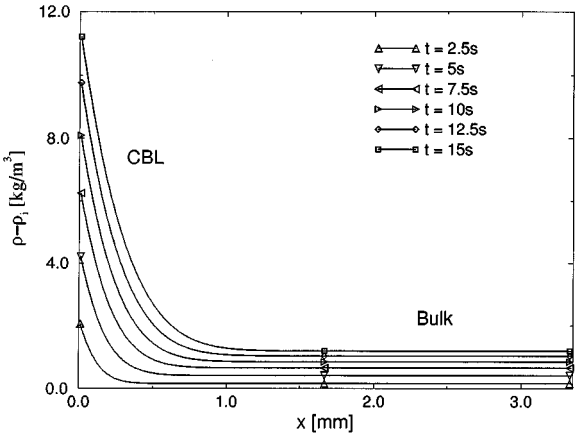


FIG. 8. The calculated density profile of the CBL near the sapphire windows during a heat pulse at $T_i \approx T_{c,x}+1$ K for different times. For $x \geqslant 1$ mm, we recover the homogeneous density rise in the bulk region. Inside the layer region, important density changes can be stated.

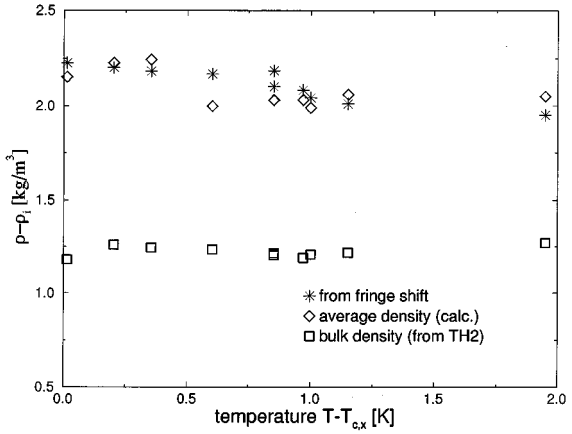


FIG. 9. Comparison of density changes after 15 s of heating for different heat pulses. The values derived from the fringe shift are compared with the average values obtained by integrating the density profile as described in Eqs. (6) and (7) and shown for one pulse in Fig. 8. Good agreement can be stated. The density rise in the bulk region remains 40–45% below the average value (see text).

temperature difference reaches the maximum value $T_i - T_{\mathrm{TH2}}$. For increasing $x$, $\delta T$ vanishes and we recover the isentropic bulk temperature $T_{\mathrm{TH2}}$. According to this temperature profile we can calculate the resulting density profile as

$$\delta\rho(x,t) = \rho(x,t) - \rho_i = \left(\frac{\partial\rho}{\partial T}\right)_{P=P_i} \delta T(x,t) + \left(\frac{\partial\rho}{\partial T}\right)_s [T_{\mathrm{TH2}}(t) - T_i]. \quad (6)$$

The second right-hand term represents the homogeneous density rise by PE compression, to which the first term is added in the layer region near the windows. We note that in this approach, the isentropic temperature rise of the bulk fluid is sufficient to calculate the temperature and density profile throughout the whole sample thickness. This temperature variation can be measured with thermistor TH2, as shown above. The density profile calculated from Eqs. (5) and (6) for the 15 s heat pulse analyzed in the preceding chapter is shown in Fig. 8. The thickness of the layer is seen to grow in time and reaches a value of order 0.7–0.8 mm at the end of the pulse. Due to the high value of the thermal expansion coefficient $(\partial\rho/\partial T)_P$ a strong density rise is obtained in this region. The calculated result compares very well with the measurement from the video image presented on Fig. 3. The layers which develop at both the bottom and the top of the sample are then extended over 15–20% of the sample thickness and may not be neglected when analyzing the fringe shift.

In order to check our analytical description of the density distribution in the sample and its influence on the fringes' phase shift, a comparison with measurements from the video images has been carried out. Introducing the temperature variation detected by TH2, thermodynamic properties of the fluid according to Abbaci and Sengers' equation of state and a diffusivity $D$ given by Jany [11], we calculated the density profile over the sample thickness outside the HBL. Integration of the phase shift of the light beam enabled the derivation of an average density rise of the profile, to be compared with the experimental value as obtained from the fringe shift. Figure 9 shows the density rise of the fluid outside the HBL as measured from the fringe displacement for the heat pulses already discussed in Figs. 7 at $t=15$ s. The values are compared with the average density rise as obtained by analyzing the stratified density profile with two CBLs at the bottom and the top of the sample [described by Eqs. (5) and (6)]. Good agreement can be stated, the average error being of order 5%. The bulk density rise given by Eq. (6) is also shown. It is seen to remain 40–45% below the average value. This result explaines the discrepancy between the isentropic coefficients $(\partial\rho/\partial T)_s$ derived from the equation of state [9] and the experimental data previously presented in Fig. 7(a). When the density rise at the windows is taken into account, the disagreement vanishes.

## III. CONCLUSIONS

In this paper we analyzed the response of a compressible fluid to an internal heat pulse in the absence of convection. The recently established theory of adiabatic heating has been confirmed by thermodynamic calculations based on measurements of the fluid's state $(P,\rho,T)$. Distinctive measurements of PE heating and diffusive heat transfer have been simultaneously carried out. The equation of state for $SF_6$ given by Abbaci and Sengers gives satisfactory results in reproducing the fluid's thermodynamic state at off-critical density. The analysis of the interference pattern has proved to be very sensitive to density inhomogeneities inside the fluid, because in contrast to the ''local'' character of temperature measurements, the interferometer integrates density variations along the optical path.

## ACKNOWLEDGMENTS

The authors want to thank the Space Shuttle crew of Columbia flight STS-65 as well as NASA and Daimler-Benz Aerospace for the faultless performance of CPF. We are very grateful to J. V. Sengers for a copy of the equation of state. We thank P. Hède for data processing as well as S. Bouquet and J. Straub for fruitful discussions.

[1] A. Onuki, H. Hao, and R. A. Ferrell, Phys. Rev. A **41**, 2256 (1990).
[2] M. Bonetti, F. Perrot, D. Beysens, and Y. Garrabos, Phys. Rev. E **49**, 4779 (1994).
[3] J. Straub, L. Eicher, and A. Haupt, Phys. Rev. E **51**, 5556 (1995).
[4] A. M. Radhwan and D. R. Kassoy, J. Eng. Math. **18**, 183 (1984).
[5] T. Fröhlich, S. Bouquet, M. Bonetti, Y. Garrabos, and D. Beysens, Phys. A **218**, 419 (1995).
[6] B. Zappoli, D. Bailly, Y. Garrabos, B. Le Neindre, P. Guenoun, and D. Beysens, Phys. Rev. A **41**, 2264 (1990).
[7] B. Zappoli and P. Carlès, Eur. J. Mech. B/Fluids **14**, 4165 (1995).
[8] P. Bravais, Institution Report No. R944063, 1995 (unpublished).
[9] A. Abbaci and J. V. Sengers, University of Maryland Technical Report No. BN1111, 1990.
[10] A. C. Michels (unpublished).
[11] P. Jany, Ph.D. thesis, Technical University of Munich, 1986.